

Crossover of rate-limiting processes in mechanochemical reactions under flow driven by applied mechanical stress

Tetsuya Yamamoto, Koji Kubota, Yu Harabuchi, Julong Jiang, and Hajime Ito

Citation: Chin. Phys. B, 2026, 35 (**7**): 078201. DOI: 10.1088/1674-1056/ae5db4
http://cpb.iphy.ac.cn; http://iopscience.iop.org/cpb

What follows is a list of articles you may be interested in

Accelerated oxygen evolution kinetics on Ir-doped $SrTiO_3$ perovskite by NH_3 plasma treatment

Li-Li Deng(邓丽丽), Xiao-Ping Ma(马晓萍), Man-Ting Lu(卢曼婷), Yi He(何弈), Rong-Lei Fan(范荣磊), and Yu Xin(辛煜)
Chin. Phys. B, 2022, 31 (**11**): 118201. DOI: 10.1088/1674-1056/ac70b1

Near-infrared photocatalysis based on upconversion nanomaterials

Xingyuan Guo(郭星原), Zhe Wang(王哲), Shengyan Yin(尹升燕), and Weiping Qin(秦伟平)
Chin. Phys. B, 2022, 31 (**10**): 108201. DOI: 10.1088/1674-1056/ac7556

Electrical and dielectric properties of $Na_{1/2}La_{1/2}Cu_3Ti_4O_{12}$ ceramics prepared by high energy ball-milling and conventional sintering

H Mahfoz Kotb, Mohamad M Ahmad
Chin. Phys. B, 2016, 25 (**12**): 128201. DOI: 10.1088/1674-1056/25/12/128201

Understanding oxygen reactions in aprotic Li-O_2 batteries

Shunchao Ma(马顺超), Yelong Zhang(张业龙), Qinghua Cui(崔清华), Jing Zhao(赵婧), Zhangquan Peng(彭章泉)
Chin. Phys. B, 2016, 25 (**1**): 018204. DOI: 10.1088/1674-1056/25/1/018204

SPECIAL TOPIC — Masao Doi: Frontiers in soft matter and polymer physics

Crossover of rate-limiting processes in mechanochemical reactions under flow driven by applied mechanical stress

Tetsuya Yamamoto[1,†], Koji Kubota[1,2], Yu Harabuchi[1], Julong Jiang[1], and Hajime Ito[1,2]

[1] *Institute for Chemical Reaction Design and Discovery (WPI-ICReDD), Hokkaido University, Sapporo* 060-8628, *Japan*
[2] *Division of Applied Chemistry, Graduate School of Engineering, Hokkaido University, Sapporo* 060-8628, *Japan*

(Received 26 February 2026; revised manuscript received 25 March 2026; accepted manuscript online 10 April 2026)

Mechanochemical organic synthesis using ball milling leverages mechanical energy to drive chemical reactions. A comprehensive understanding of the underlying reaction kinetics is essential for the continuous development of mechanochemical synthesis. However, the rate-limiting processes of mechanochemical reactions remain poorly understood because molecular behavior at interfacial length scales is still largely unknown. We have theoretically predicted that mechanochemical reactions of two solid reactants lead to the formation of a product-rich phase at their interface due to the instability arising from the immiscibility of product and reactant solids and that the applied mechanical stress accelerates the diffusion of reactants through the product-rich layer by decreasing the thickness of this layer. To shed light on the rate-limiting processes governing such mechanochemical reactions, we develop here a scaling theory. This theory predicts that the rate-limiting process depends on the thickness of the product-rich layer and can therefore change over time. Unlike conventional solution-based reactions, the crossover between regimes of rate-limiting processes is influenced not only by the diffusion length but also by the extent of reactant dissolution into the product-rich layer and the magnitude of the applied mechanical stress. The model developed in this study provides a fundamental framework for a deeper understanding of mechanochemical organic reactions occurring during ball milling.

Keywords: mechanochemistry, rate-limiting process, scaling theory, ball-milling, reaction kinetics

PACS: 82.45.Jn, 82.20.–w, 83.80.Jx

DOI: 10.1088/1674-1056/ae5db4 **CSTR:** 32038.14.CPB.ae5db4

1. Introduction

Mechanochemical organic synthesis using ball milling requires little or no organic solvent and has attracted significant attention as an efficient, energy-saving, and ecofriendly alternative to conventional solution-based approaches that rely on organic solvents. A wide range of organic reactions can be performed efficiently using ball milling.[1–7] Strong mechanical agitation by ball milling grinds the reactants, reagents, and catalysts (Fig. 1(a)). Since no solvent is required under mechanochemical conditions, the reactants are used in their native physical states, which can either be solid or liquid, depending on the compounds and reaction conditions.[8,9] A comprehensive understanding of reaction kinetics under mechanochemical conditions is essential for advancing techniques based on mechanochemical synthesis. Identifying the rate-limiting processes is the first step in understanding the kinetics of chemical reactions.[10] However, the rate-limiting processes of mechanochemical reactions remain poorly understood owing to the inherent complexity arising from the fact that chemical reactions at molecular length scales are accelerated by macroscopic mechanics,[11] and that molecular dynamics in systems composed of multiple phases are involved.

The processes involved in mechanochemical reactions range from macroscopic (solid particles) to microscopic (molecular) levels (Fig. 1).[11] At the macroscopic level, mechanical agitation drives the motion of metal balls and solid reactants, as well as the fragmentation of the reactants (Fig. 1(a)). Theoretically, these processes have been studied using the physics of granular materials[12–14] and by modeling them as Poisson processes.[15] At the molecular level, the reactants transform into the product (Fig. 1(b)). It is straightforward to think that the applied mechanical force can directly activate the starting materials and catalysts, thereby decreasing the activation energy of the reactions.[11–13] Indeed, the impact of applied tension on the reactions of polymeric compounds has been widely studied.[16–21] Polymer chains are considered to induce and control force transduction so that functional units (mechanophores) can be activated. Theoretically, the activation force is predicted using density functional theory (DFT)-based quantum chemical calculations, in which the work done by displacements[22,23] or externally applied forces on pairs of terminal atoms[24] or functional groups[21] is considered. In contrast, the detailed role of mechanical stress in mechanochemical reactions involving small molecules by ball milling remains unclear, except for a few specifically designed systems,[25–27] probably because the processes at intermediate

†Corresponding author. E-mail: tyamamoto@icredd.hokudai.ac.jp

© 2026 Chinese Physical Society and IOP Publishing Ltd. All rights, including for text and data mining, AI training, and similar technologies, are reserved.

length scales between the macroscopic and molecular limits remain poorly understood.

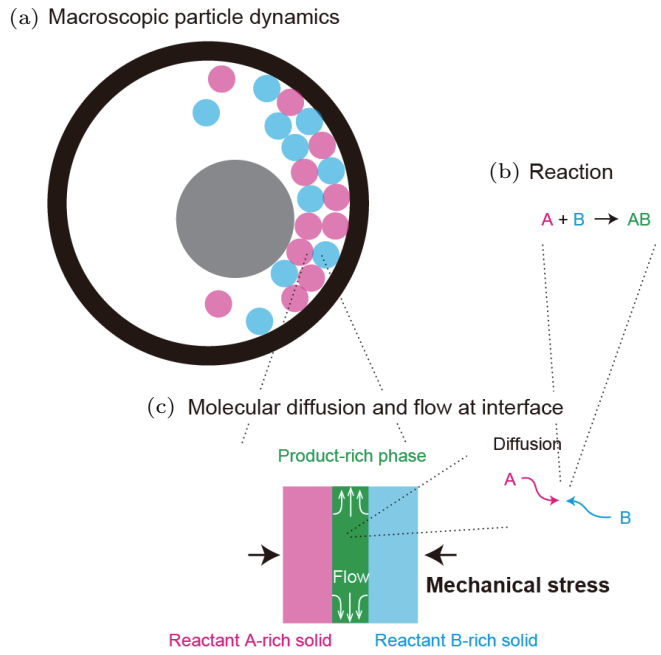


Fig. 1. Mechanochemical organic synthesis by ball milling. (a) Mechanochemical synthesis is performed by mechanical agitation of solid reactants (magenta and cyan circles) and metal balls (gray circle). (b) At the molecular level, reactants A and B transform into product AB. (c) Mechanochemical reactions occur at the interfaces between reactant solids (magenta and cyan slabs), producing a product-rich layer (green) at these interfaces. The applied mechanical stress by the metal balls drives material flow in the product-rich phase. Reactant molecules A and B diffuse in the product-rich layer and undergo chemical reactions when they meet.

Mechanochemical reactions involving solid reactants occur at the interface (Fig. 1(c)). Molecular dynamics (MD) simulations have predicted that the plasticity of colliding solid reactant particles plays a key role in the mixing of reactants.[28,29] However, MD simulations are limited to short timescales before chemical reactions occur. We previously developed a theory combining the Landau theory for phase transition with the Onsager theory for irreversible processes, which predicts that mechanochemical reactions of two solid reactants produce a product-rich phase at their interface due to instabilities arising from the immiscibility of products and reactants (green layer in Fig. 1(c)).[30] The theory also predicts that the dissolution of reactant molecules into the product-rich layer regulates the kinetics of mechanochemical reactions.[30] Interestingly, adding a small volume of solvent to the system enhances the reactivity of solid reactants,[31] probably because the solvent wets the surfaces of reactant solids and acts as a plasticizer for the product-rich layer. Under these conditions, the applied mechanical stress drives material flow, increasing the concentration gradient of the reactants in the product-rich layer by decreasing its thickness (white arrows in Fig. 1(c)).[32] This mechanical effect accelerates diffusion-limited reactions, whose rates depend on the concentration gradient of the reactants, but does not influence reaction-limited processes, whose rates depend on the local reactant concentrations. However, the previously proposed theory could not predict the factors determining the rate-limiting processes of mechanochemical reactions.

To shed light on the rate-limiting processes of mechanochemical reactions, we develop a theory to study the conditions under which mechanochemical reactions are limited by diffusion or by reaction. In conventional solution-based reactions, the rate-limiting processes are determined by the diffusion length, which is the distance a reactant can diffuse before reacting.[33] The proposed theory predicts that, in mechanochemical reactions, the rate-limiting process depends on the thickness of the product-rich layer and the system size, and can therefore change over time. In the diffusion-limited regime, chemical reactions occur as soon as the reactants meet because the intrinsic reaction is faster than diffusion. In the reaction-limited regime, diffusion of molecules is faster than the reaction; thus, the volume fractions of the reactants and products are determined by thermodynamic equilibrium conditions due to the multiphase nature of the system. There is also a "marginal" regime, in which the rate-limiting process is the reaction, but a reactant A molecule penetrates the reactant B-rich solid phase (and vice versa) only up to the diffusion length. The crossover between reaction regimes is determined not only by the diffusion length but also by the extent of dissolution of reactant molecules into the product-rich layer and the applied mechanical stress. Although the present analysis is limited to mesoscopic interfacial dynamics, it provides a basis for understanding the rate-limiting process of mechanochemical reactions by bridging microscopic and macroscopic dynamics.

2. Scaling theory for kinetics of mechanochemical reactions

We develop a scaling theory to analyze the rate-limiting processes in mechanochemical reactions by extending our previous theoretical studies.[30,32] This theory considers a simple mechanochemical reaction between two solid reactants, A and B, that forms a product AB ($\mathrm{A}+\mathrm{B}\rightarrow\mathrm{AB}$). We focus on the interfacial region between the two solid reactants where mechanochemical reactions occur. The coordinate system is set such that the x–y plane lies at the interface between the solid reactants, and the z axis is normal to this plane (Fig. 2(a)). The system is described by the volume fractions, $\psi_{\mathrm{A}}(z)$, $\psi_{\mathrm{B}}(z)$, and $\psi_{\mathrm{AB}}(z)$, of the reactants and products. Subscripts A, B, and AB represent the quantities of reactants A and B and product AB, respectively. For simplicity, we consider cases in which the diffusion constants and thermodynamic properties of the two reactants are equal, and the volume per product molecule AB is the sum of the volumes per

molecule of reactants A and B. In this case, the volume fractions of reactants A and B are symmetric with respect to the x–y plane, $\psi_{\rm A}(z) = \psi_{\rm B}(-z)$. Thus, we analyze only half of the system, $z > 0$. By neglecting the small volume of added solvents, the system is occupied by the reactants or the product (incompressibility condition)

$$\psi_{\rm A}(z) + \psi_{\rm B}(z) + \psi_{\rm AB}(z) = 1. \tag{1}$$

The volume fractions of A and B follow reaction–diffusion equations:[34]

$$\frac{\partial}{\partial t}\psi_{\rm A}(z) = D_{\rm A}\frac{\partial}{\partial z}\left(\psi_{\rm A}(z)\frac{\partial}{\partial z}\frac{\mu_{\rm A}(\psi_{\rm A},\psi_{\rm B})}{k_{\rm B}T}\right) - k\psi_{\rm A}(z)\psi_{\rm B}(z), \tag{2}$$

$$\frac{\partial}{\partial t}\psi_{\rm B}(z) = D_{\rm B}\frac{\partial}{\partial z}\left(\psi_{\rm B}(z)\frac{\partial}{\partial z}\frac{\mu_{\rm B}(\psi_{\rm A},\psi_{\rm B})}{k_{\rm B}T}\right) - k\psi_{\rm A}(z)\psi_{\rm B}(z), \tag{3}$$

where $\mu_{\rm A}(\psi_{\rm A},\psi_{\rm B})$ and $\mu_{\rm B}(\psi_{\rm A},\psi_{\rm B})$ are the chemical potentials of A and B, respectively. $D_{\rm A}$ and $D_{\rm B}$ are the diffusion constants of reactants A and B, respectively. k is the reaction rate constant. The volume fraction of the product $\psi_{\rm AB}(z)$ is determined by the incompressibility condition (Eq. (1)). Equations (2) and (3) imply that the chemical potentials, rather than the volume fractions, are continuous throughout the system.

The reactant B solid is stable only when the volume fraction $\psi_{\rm B}(z)$ is larger than the binodal value, $\psi_{\rm B}(z) > \psi_{\rm B2}$, and a phase rich in products or reactant A is stable when the volume fraction is smaller than another binodal value, $\psi_{\rm B}(z) < \psi_{\rm B1}$.[34–36] The volume fraction between the two binodal values, $\psi_{\rm B1} < \psi_{\rm B}(z) < \psi_{\rm B2}$, is unstable. The binodal volume fractions, $\psi_{\rm B1}$ and $\psi_{\rm B2}$, can be determined experimentally. In our previous study, we derived $\psi_{\rm B1}$ and $\psi_{\rm B2}$ as functions of the immiscibility parameter using the mean-field approximation.[30] The volume fraction $\psi_{\rm B}(z)$ of reactant B thus exhibits a discontinuity between $\psi_{\rm B1}$ and $\psi_{\rm B2}$ at $z = h(t)$ (Figs. 2(b)–2(d)). This discontinuity is accompanied by a corresponding jump in the volume fraction $\psi_{\rm A}(z)$ of reactant A between the binodal values $\psi_{\rm A1}$ and $\psi_{\rm A2}$ at the same position. Note that the chemical potentials are equal at the binodal values, $\mu_{\rm A}(\psi_{\rm A1},\psi_{\rm B1}) = \mu_{\rm A}(\psi_{\rm A2},\psi_{\rm B2})$ and $\mu_{\rm B}(\psi_{\rm A1},\psi_{\rm B1}) = \mu_{\rm B}(\psi_{\rm A2},\psi_{\rm B2})$, ensuring continuity of the chemical potentials at $z = h(t)$ (local equilibrium). The region $z > h(t)$ is predominantly occupied by reactant B and is thus identified as the reactant-B-rich solid phase. The discontinuity in the volume fraction at $z = h(t)$ results from the instability arising from the immiscibility between the product and reactant solids, and the region $0 < z < h(t)$ thus forms a distinct product-rich phase.

A small volume of solvent added to the system can wet the surfaces of the solid reactant particles and act as a plasticizer in the product-rich phase.[31] For simplicity, we treat the reactant-rich solid phases as rigid bodies and the product-rich phase as a viscous fluid. The applied mechanical stress $\sigma_\perp$ drives flow in the product-rich phase. We here consider cases in which the relaxation time of the product-rich phase is faster than the frequency of the metal ball motions so that the applied mechanical stress is assumed to be static. The material flow decreases the thickness of the product-rich phase at a speed

$$v(t) = \frac{8}{3}\frac{\sigma_\perp}{\eta_{\rm AB} r_0^2}h^3(t), \tag{4}$$

where $\eta_{\rm AB}$ is the viscosity of the product-rich phase and r_0 is the radius of the interfacial region. Equation (4) is derived by solving the Stokes equation under the lubrication approximation.[32,35] The thickness $h(t)$ of the product-rich phase depends on the reaction rate $S(t)$ and material flow $v(t)$

$$\frac{\rm d}{{\rm d}t}h(t) = \frac{S(t)}{1-\psi_{\rm A1}-\psi_{\rm B1}} - v(t). \tag{5}$$

The reaction rate $S(t)$ is defined by the volume of reactants converted to product per unit time and area, and its form depends on the rate-limiting process of the reaction.

The reaction can occur throughout the entire system of size $L(t)$ in the reaction-limited regime. The thickness $L(t)$ of the system evolves according to the following equation:

$$\frac{\rm d}{{\rm d}t}L(t) = -v(t). \tag{6}$$

The volume $V_{\rm ex}(t)$ of material is excluded from the interfacial region between the solid reactants by the material flow under the applied mechanical stress, as described by Eq. (4). Mass conservation can then be expressed as follows:

$$\frac{\rm d}{{\rm d}t}(V_{\rm ex}(t) + \pi r_0^2 L(t)) = 0. \tag{7}$$

2.1. Diffusion-limited regime

In the diffusion-limited regime, the reactant molecules A and B react immediately upon meeting at $z = 0$ (Fig. 2(b)). Reactant A molecules do not penetrate the region defined by $z > 0$, and the volume fraction of reactant B molecules at the interface $z = 0$ vanishes, $\psi_{\rm B}(0) = 0$. In the low-temperature limit, the volume fraction $\psi_{\rm B}(z)$ of reactant B molecules in the product-rich phase is small. In this case, the chemical potential of reactant B assumes an asymptotic form expressed as $\mu_{\rm B} = k_{\rm B}T\log\psi_{\rm B}(z)$. Solving Eq. (3) in the steady state, the volume fractions of reactants have the form $\psi_{\rm A}(z) = 0$ and $\psi_{\rm B}(z) \approx \psi_{\rm B1}^{\rm d} z/h(t)$ for $0 < z < h(t)$. The superscript 'd' indicates the binodal value in the diffusion-limited regime (binary mixture of reactant B and product). The flux $J_{\rm B}(z)$ represents the volume of reactant B molecules crossing a unit area per unit time

$$J_{\rm B}(z) = -D_{\rm B}\psi_{\rm B}(z)\frac{\partial}{\partial z}\mu_{\rm B}(\psi_{\rm A},\psi_{\rm B}). \tag{8}$$

In the diffusion-limited regime, the reaction rate $S(t)(=-J_{\rm B}(0))$ is equal to the flux of reactant B reaching $z=0$. Substituting the steady-state profile, the reaction rate has the form

$$S(t)=D_{\rm B}\frac{\psi^{\rm d}_{\rm B1}}{h(t)}. \tag{9}$$

The diffusion of reactant molecules occurs only within the region between the two solid reactants.

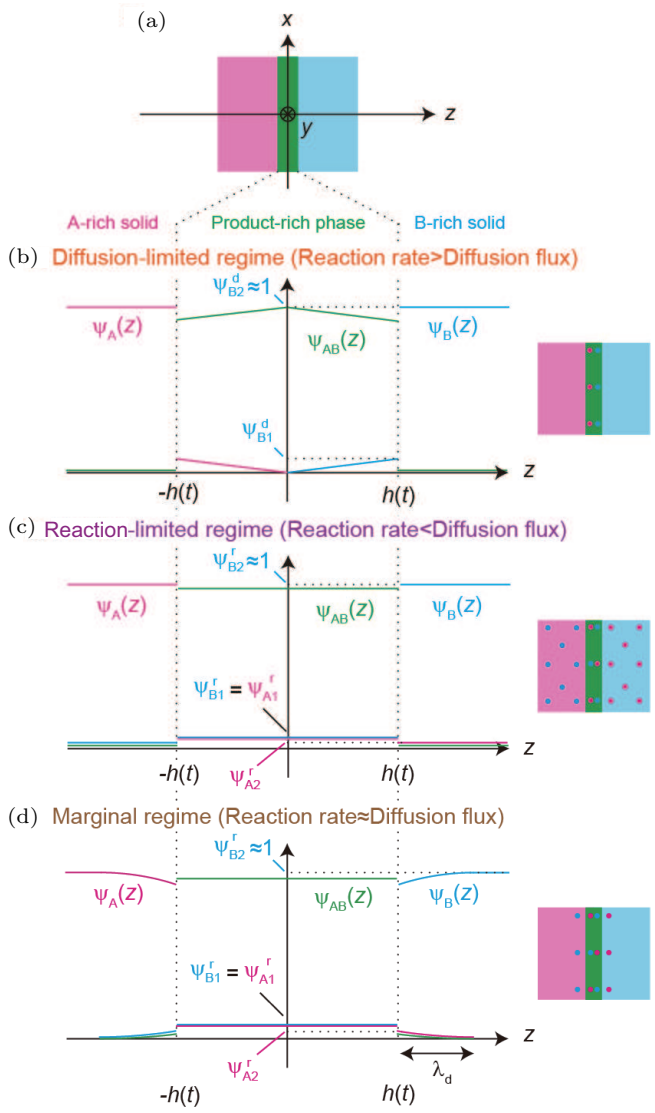


Fig. 2. Volume fraction profiles of reactants. (a) Schematic showing the coordinate system, where the x–y plane is located at the mid-plane of the product-rich layer (green) and the z axis is normal to the plane. The volume fractions of reactants A (magenta) and B (cyan) as well as product AB (green) are presented as functions of position z for the diffusion-limited (b), reaction-limited (c), and marginal regimes (d).

2.2. Reaction-limited regime

In the reaction-limited regime, the diffusion of reactant A and B molecules is so fast that the volume fractions of reactants and products are determined using thermodynamic equilibrium conditions (Fig. 2(c)). The volume fractions of the reactant molecules in the two reactant-rich solid phases and the product-rich phase are maintained at the binodal values, and the reaction primarily changes the thickness of these phases. Thus, the reaction rate $S(t)$ is expressed as follows:

$$\begin{aligned}S(t) &= k\psi^{\rm r}_{\rm A1}\psi^{\rm r}_{\rm B1}h(t)+k\psi^{\rm r}_{\rm A2}\psi^{\rm r}_{\rm B2}(L(t)-h(t))\\ &\quad +k\psi^{\rm r}_{\rm A1}\psi^{\rm r}_{\rm B1}\frac{V_{\rm ex}(t)}{\pi r_0^2}.\end{aligned} \tag{10}$$

The superscript 'r' denotes the binodal value in the reaction-limited regime (ternary mixture of A, B, and AB). The first, second, and third terms in Eq. (10) correspond to the reaction rates in the product-rich phase, reactant-rich solid phase, and the volume flown out from the region between the reactant-rich solid phases, respectively. At first glance, one may think that the reaction rate $S(t)$ depends on the flow via $h(t)$, $L(t)$, and $V_{\rm ex}(t)$, see Eqs. (5)–(7). However, by taking the time derivative of both sides of Eq. (10), we derive the relationship

$$\frac{\rm d}{{\rm d}t}S(t)=\frac{k(\psi^{\rm r}_{\rm A1}\psi^{\rm r}_{\rm B1}-\psi^{\rm r}_{\rm A2}\psi^{\rm r}_{\rm B2})}{1-\psi^{\rm r}_{\rm A1}-\psi^{\rm r}_{\rm B1}}S(t). \tag{11}$$

Eq. (11) shows that, in the reaction-limited regime, the reaction rate $S(t)$ is independent of flow.

2.3. Marginal regime

In the marginal regime, the product-rich phase remains in thermodynamic equilibrium, while reactant A molecules penetrate the reactant B-rich solid phase only over the diffusion length (Fig. 2(d))

$$\lambda_{\rm d}=\sqrt{\frac{D_{\rm A}}{k}}. \tag{12}$$

In this case, the reaction rate has the form

$$S(t)=k\psi^{\rm r}_{\rm A1}\psi^{\rm r}_{\rm B1}h(t)+k\psi^{\rm r}_{\rm A2}\psi^{\rm r}_{\rm B2}\lambda_{\rm d}+k\psi^{\rm r}_{\rm A1}\psi^{\rm r}_{\rm B1}\frac{V_{\rm ex}(t)}{\pi r_0^2}. \tag{13}$$

By taking the time derivative of both sides of Eq. (13), we derive the relationship

$$\frac{\rm d}{{\rm d}t}S(t)=\frac{k\psi^{\rm r}_{\rm A1}\psi^{\rm r}_{\rm B1}}{1-\psi^{\rm r}_{\rm A1}-\psi^{\rm r}_{\rm B1}}S(t). \tag{14}$$

Thus, the reaction rate $S(t)$ does not depend on the flow in the marginal regime. The only difference between the reaction-limited and marginal regimes is the distribution of reactant A molecules within the reactant B-rich solid phase and vice versa. Because the binodal values in the marginal regime are identical to those in the reaction-limited regime, we use the same superscript 'r'.

The time evolution of the system is derived by solving Eqs. (5) and (6), with the flow fields given by Eq. (4). The reaction rates $S(t)$ in the diffusion-limited, reaction-limited, and marginal regimes are derived using Eqs. (9), (11), and (14), respectively. The reaction regime is determined by the minimum among these reaction rates.

Table 1. Characteristic length scale, time scale, and mechanical stress used in the present theory and the volumefraction ratios.

Symbol	Meaning	Expression	Used value
$\lambda_{\rm d}$	Diffusion length	$\sqrt{D_{\rm A}/k}$	–
$\frac{1}{\tau_{\rm p}}$	Inverse reaction time	$\frac{k\psi^{\rm r}_{\rm A1}\psi^{\rm r}_{\rm B1}}{1-\psi^{\rm r}_{\rm A1}-\psi^{\rm r}_{\rm B1}} \approx k\psi^{\rm r}_{\rm A1}\psi^{\rm r}_{\rm B1}$	–
$\sigma_{\rm p}$	Mechanical stress scale	$\frac{3}{8}\frac{\eta_{\rm AB}}{\tau_{\rm p}}\frac{r_0^2}{\lambda_{\rm d}^2}$	–
α	Volume fraction ratio of phases	$\frac{\psi^{\rm r}_{\rm A2}\psi^{\rm r}_{\rm B2}}{\psi^{\rm r}_{\rm A1}\psi^{\rm r}_{\rm B1}} \approx \frac{\psi^{\rm r}_{\rm A2}}{(\psi^{\rm r}_{\rm A1})^2}$	0.01
β	Volume fraction ratio of regimes	$\frac{\psi^{\rm d}_{\rm B1}}{\psi^{\rm r}_{\rm A1}\psi^{\rm r}_{\rm B1}}\frac{1-\psi^{\rm r}_{\rm A1}-\psi^{\rm r}_{\rm B1}}{1-\psi^{\rm d}_{\rm B1}} \approx \frac{\psi^{\rm d}_{\rm B1}}{(\psi^{\rm r}_{\rm B1})^2}$	10.0

The present theory is formulated in terms of the characteristic length scale $\lambda_{\rm d}$, time scale $\tau_{\rm p}$, and mechanical stress $\sigma_{\rm p}$ as well as the volume-fraction ratios α and β (Table 1). The ratio β is estimated to be large because $\psi^{\rm r}_{\rm A1} \approx \psi^{\rm r}_{\rm B1} \approx \psi^{\rm d}_{\rm B1}/2$. The ratio α depends on the extent to which reactant A dissolves into the reactant-B-rich solid (and vice versa), relative to dissolution of these molecules in the product-rich phase. The reaction rate (per unit area) scales as

$$S_{\rm p} = \frac{(1-\psi^{\rm r}_{\rm A1}-\psi^{\rm r}_{\rm B1})\lambda_{\rm d}}{\tau_{\rm p}}. \tag{15}$$

3. Regime diagram without applied mechanical stress

In the absence of applied mechanical stress ($v = 0$), the system size remains constant, $L(t) = L_0$ (Eq. (6)), where $L_0 (= L(0))$ represents the initial system size. Our theory predicts that the rate-limiting process depends on the thickness $h(t)$ of the product-rich phase and the system size L_0 (Fig. 3(a)). Because the thickness $h(t)$ increases over time, the rate-limiting process can change as the reaction proceeds. We identify four types of trajectories: I. For $L_0 > L_2^*$, the reaction begins in the marginal regime and subsequently enters the diffusion-limited regime (black arrow in Fig. 3(a)). II. For $L_1^* < L_0 < L_2^*$, the reaction sequentially passes through the marginal, reaction-limited, and diffusion-limited regimes (cyan arrows in Fig. 3(a)). III. For $\lambda_{\rm d} < L_0 < L_1^*$, the reaction starts in the marginal regime and then shows a crossover to the reaction-limited regime (magenta arrow in Fig. 3(a)). IV. For $L_0 < \lambda_{\rm d}$, the kinetics remain reaction-limited over the entire reaction time. The explicit expressions for L_1^* and L_2^* are summarized in Table 2, and their derivations are provided in the supplementary information (SI).

Marginal/diffusion-limited, marginal/reaction-limited, and reaction-limited/diffusion-limited crossovers occur when the thicknesses of the corresponding product-rich layers are $h_{\rm md0}$, $h_{\rm mr0}$, and $h_{\rm rd0}$, respectively (Fig. 3(a)). The expressions for the thicknesses of the product-rich layers and the corresponding times are summarized in Tables 3 and 4. The rate-limiting processes are determined not only by the diffusion length $\lambda_{\rm d}$ but also by the parameters α and β, which represent the extent of reactant molecule dissolution in the product-rich phase, unlike in conventional solution-based reactions.

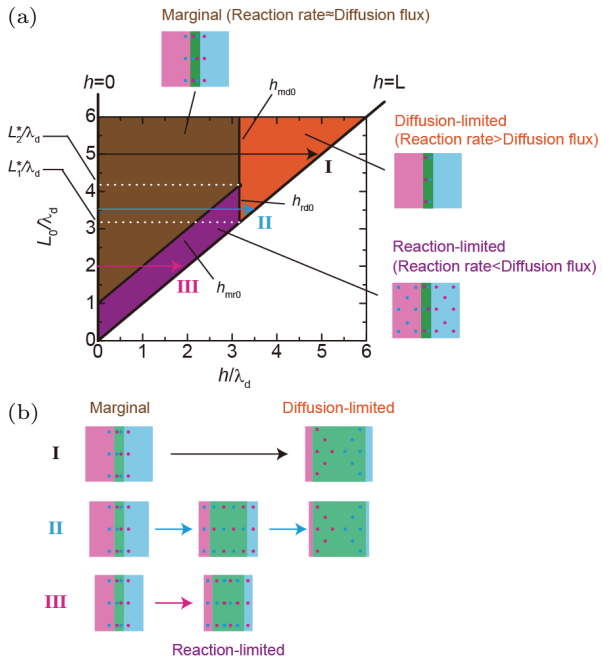


Fig. 3. Regime diagram without material flow. (a) Regime diagram of rate-limiting processes of mechanochemical reactions with respect to the product-rich layer thickness $h(t)$ and system size L_0. The diagram was constructed using the expressions in Tables 2–4 with $\alpha = 0.01$ and $\beta = 10.0$. The diffusion-limited, reaction-limited, and marginal regimes are shown in orange, purple, and brown, respectively. Without flow in the product-rich layer, the system size L_0 remains constant, whereas the thickness $h(t)$ of the product-rich layer increases over time (trajectories indicated by black, cyan, and magenta arrows). The marginal/diffusion-limited, marginal/reaction-limited, and reaction-limited/diffusion-limited crossover boundaries are denoted by $h_{\rm md0}$, $h_{\rm mr0}$, and $h_{\rm rd0}$, respectively. The sequence of crossovers experienced by the system depends on L_0 with three thresholds $\lambda_{\rm d}$, L_1^*, and L_2^*. (b) Schematic illustration of the crossover sequences corresponding to the black, cyan, and magenta trajectories shown in panel (a).

4. Reaction rate without applied mechanical stress

The expressions for the reaction rate and thickness of the product-rich layer in each regime are provided in Tables 5 and

6, and their derivations are provided in the SI. In the marginal regime, the reaction rate $S_{\mathrm{m}}(t)$ increases over time as

$$S_{\mathrm{m}}(t) = k\psi^{\mathrm{r}}_{\mathrm{A2}}\psi^{\mathrm{r}}_{\mathrm{B2}}\lambda_{\mathrm{d}}\,\mathrm{e}^{\frac{t}{\tau_{\mathrm{p}}}}, \tag{16}$$

because the reaction occurs uniformly in the product-rich layer (black line in Fig. 4(a)). In the diffusion-limited regime, the reaction rate $S_{\mathrm{d}}(t)$ decreases over time as

$$S_{\mathrm{d}}(t) = D_{\mathrm{B}}\frac{\psi^{\mathrm{d}}_{\mathrm{B1}}}{\sqrt{h^2_{\mathrm{md0}} + \dfrac{2\beta\lambda_{\mathrm{d}}^2(t-t_{\mathrm{md0}})}{\tau_{\mathrm{p}}}}}. \tag{17}$$

Because diffusion of reactants in the product-rich layer decelerates as the thickness $h(t)$ of this layer increases (black line in Fig. 4(a); see Tables 2 and 3 for h_{md0} and t_{md0}), the reaction rate exhibits a maximum S_{md0} at the crossover between the marginal and diffusion-limited regimes. This non-monotonic behavior results from the fact that the reaction rate is proportional to the inverse of the thickness of the product-rich layer in the diffusion-limited regime, whereas in the marginal regime it is proportional to the thickness of this layer.

The non-monotonicity in the reaction rate may be experimentally accessible unless the characteristic time t_{md0} at the marginal/diffusion-limited crossover is either too short or too long compared with the experimental time scale. The characteristic time t_{md0} is given by

$$t_{\mathrm{md0}} = \tau_{\mathrm{p}}\log\left(\frac{1}{2} + \sqrt{\frac{1}{4} + \frac{\beta}{\alpha^2}}\right). \tag{18}$$

Table 2. Threshold system sizes, L_1^* and L_2^*, that determine changes in trajectory type in the absence of applied mechanical stress. The derivations are provided in SI.

Symbol	Trajectories	Expression	SI
λ_{d}	III–IV	$\sqrt{D_{\mathrm{A}}/k}$	–
L_1^*	II–III	$\sqrt{\beta}\lambda_{\mathrm{d}}$	S25
L_2^*	I–II	$\alpha\lambda_{\mathrm{d}}\left(\sqrt{\frac{1}{4}+\frac{\beta}{\alpha^2}}-\frac{1}{2}\right)+\lambda_{\mathrm{d}}$	S24

Table 3. Product-rich layer thickness $h(t)$ of at the regime crossover points in the absence of applied mechanical stress. The derivations are provided in SI.

Symbol	Regimes	Expression	SI
h_{md0}	Marginal/diffusion-limited	$\alpha\lambda_{\mathrm{d}}\left(\sqrt{\frac{1}{4}+\frac{\beta}{\alpha^2}}-\frac{1}{2}\right)$	S12
h_{mr0}	Marginal/reaction-limited	$L_0-\lambda_{\mathrm{d}}$	S16
h_{rd0}	Reaction-limited/diffusion-limited	$\dfrac{\sqrt{4\beta(1-\alpha)\lambda_{\mathrm{d}}^2+(\alpha L_0)^2}-\alpha L_0}{2(1-\alpha)}$	S20

Table 4. Characteristic time at the crossovers between regimes in the absence of applied mechanical stress. The derivations are provided in SI.

Symbol	Regimes	Expression	SI
t_{md0}	Marginal/diffusion-limited	$\tau_{\mathrm{p}}\log\left(\frac{1}{2}+\sqrt{\frac{1}{4}+\frac{\beta}{\alpha^2}}\right)$	S13
t_{mr0}	Marginal/reaction-limited	$\tau_{\mathrm{p}}\log\left(1+\frac{L_0-\lambda_{\mathrm{d}}}{\alpha\lambda_{\mathrm{d}}}\right)$	S17
t_{rd0}	Reaction-limited/diffusion-limited	$t_{\mathrm{mr0}}+\frac{\tau_{\mathrm{p}}}{1-\alpha}\log\left\{\frac{\sqrt{4\beta(1-\alpha)\lambda_{\mathrm{d}}^2+(\alpha L_0)^2}-\alpha L_0}{2[L_0-(1-\alpha)\lambda_{\mathrm{d}}]}\right\}$	S21

Table 5. Reaction rate in the reaction-limited, diffusion-limited, and marginal regimes in the absence of material flow driven by applied mechanical stress. The derivation of these expressions is given in the SI. h_{d0} and t_{d0} are the thicknesses of the product-rich layer and time at which the system enters the diffusion-limited regime. $h_{\mathrm{d0}}=h_{\mathrm{md0}}$ and $t_{\mathrm{d0}}=t_{\mathrm{md0}}$ for the marginal/diffusion-limited crossover; $h_{\mathrm{d0}}=h_{\mathrm{rd0}}$ and $t_{\mathrm{d0}}=t_{\mathrm{rd0}}$ for the reaction-limited/diffusion-limited crossover.

Symbol	Regime	Expression	SI
$S_{\mathrm{r}}(t)$	Reaction-limited ($L_0>\lambda_{\mathrm{d}}$)	$k\psi^{\mathrm{r}}_{\mathrm{A2}}\psi^{\mathrm{r}}_{\mathrm{B2}}\lambda_{\mathrm{d}}\exp\left[\frac{t_{\mathrm{mr0}}}{\tau_{\mathrm{p}}}+(1-\alpha)\frac{t-t_{\mathrm{mr0}}}{\tau_{\mathrm{p}}}\right]$	S18
$S_{\mathrm{d}}(t)$	Diffusion-limited	$D_{\mathrm{B}}\dfrac{\psi^{\mathrm{d}}_{\mathrm{B1}}}{\sqrt{h^2_{\mathrm{d0}}+\frac{2\beta\lambda_{\mathrm{d}}^2(t-t_{\mathrm{d0}})}{\tau_{\mathrm{p}}}}}$	S15, S23
$S_{\mathrm{m}}(t)$	Marginal	$k\psi^{\mathrm{r}}_{\mathrm{A2}}\psi^{\mathrm{r}}_{\mathrm{B2}}\lambda_{\mathrm{d}}\exp\left(\frac{t}{\tau_{\mathrm{p}}}\right)$	S10

Table 6. Thickness of the product-rich phase in the reaction-limited, diffusion-limited, and marginal regimes in the absence of the material flow driven by applied mechanical stress. The derivation of these expressions is given in the SI. $h_{\rm d0}$ and $t_{\rm d0}$ are the thicknesses of the product-rich layer and time at which the system enters the diffusion-limited regime.

Symbol	Regime	Expression	SI
$h_{\rm r}(t)$	Reaction-limited	$h_{\rm mr0}+\frac{\alpha}{1-\alpha}\lambda_{\rm d}\exp\left(\frac{t_{\rm mr0}}{\tau_{\rm p}}\right)\left[\exp\left((1-\alpha)\frac{t-t_{\rm mr0}}{\tau_{\rm p}}\right)-1\right]$	S19
$h_{\rm d}(t)$	Diffusion-limited	$\sqrt{h_{\rm d0}^2+\frac{2\beta\lambda_{\rm d}^2(t-t_{\rm d0})}{\tau_{\rm p}}}$	S14,S22
$h_{\rm m}(t)$	Marginal	$\alpha\lambda_{\rm d}\left(\exp\left(\frac{t}{\tau_{\rm p}}\right)-1\right)$	S11

Equation (18) is derived by enforcing continuity of the reaction rate and the thickness of the product-rich layer at the marginal/diffusion-limited crossover (see Table 4). The crossover time $t_{\rm md0}$ has asymptotic forms $\beta\tau_{\rm p}/\alpha^2$ for $\frac{\beta}{\alpha^2}\ll 1$ and $\frac{\tau_{\rm p}}{2}\log\frac{\beta}{\alpha^2}$ for $\frac{\beta}{\alpha^2}\gg 1$. This implies that, if the dissolution of reactant A into the reactant B-rich solid is strongly hindered relative to its dissolution in the product-rich phase, $\psi^{\rm r}_{\rm A2}/\psi^{\rm r}_{\rm A1}\ll\sqrt{\psi^{\rm d}_{\rm B1}}$, the reaction becomes diffusion-limited only on long time scales, near completion. The reaction rate thus increases for most of the time. In contrast, when the volume fraction of reactant A dissolved into the reactant B-rich solid is comparatively large relative to that in the product-rich phase, $\psi^{\rm r}_{\rm A2}/\psi^{\rm r}_{\rm A1}\gg\sqrt{\psi^{\rm d}_{\rm B1}}$, the marginal regime persists only on short time scales. The reaction rate thus decreases for most of the time.

5. Reaction rate with applied mechanical stress

For systems with very large size $L_0\to\infty$, the mechanochemical reaction starts in the marginal regime and then undergoes a crossover to the diffusion-limited regime. In the absence of applied mechanical stress, the reaction rate decreases over time in the diffusion-limited regime (black line in Fig. 4(a)). With applied mechanical stress, the reaction rate decreases only slightly after the marginal/diffusion-limited crossover and then becomes constant (magenta and light green lines in Fig. 4(a)). Thus, the applied mechanical stress accelerates the mechanochemical reaction in the diffusion-limited regime. This acceleration arises because the stress-driven material flow decreases the thickness of the product-rich layer, thereby increasing the diffusive flux of reactant molecules through this layer.[32] A new finding in our present study is that the characteristic time at the marginal/diffusion-limited crossover increases with increasing applied mechanical stress (see black, magenta, and light green lines in Fig. 4(a)).

Quantitatively, Eq. (4) suggests that the stress-driven material flow is not significant on short time scales, when $h(t)\approx 0$. In this short-time regime, Eqs. (16) and (17) are effective. On long time scales, the material flow becomes significant, and the increase in the thickness of the product-rich layer owing to the mechanochemical reaction is balanced by its decrease due to the material flow

$$S(t)\approx v(t)\,, \tag{19}$$

See Eq. (5). The time at which this crossover between the two time regimes occurs is denoted as $t_{\rm c}$.

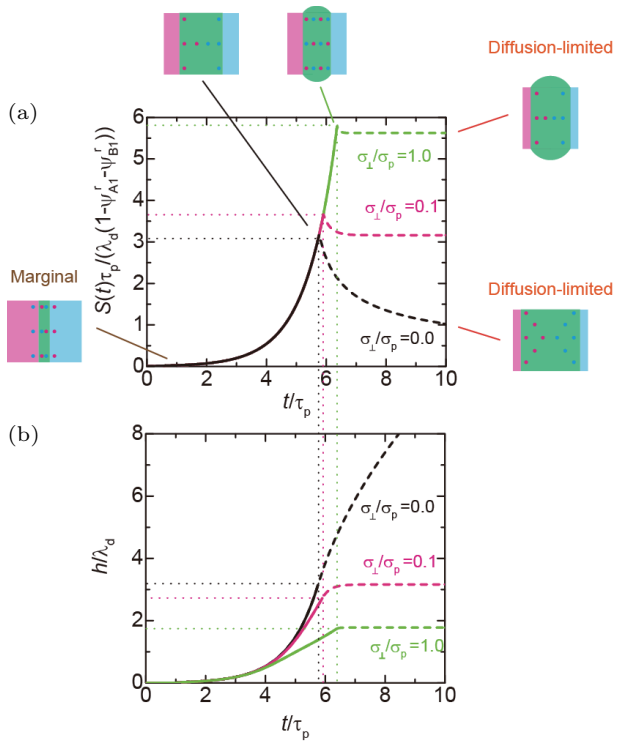


Fig. 4. Reaction rate vs. time. The reaction rate $S(t)$ (rescaled by the scale $S_{\rm p}$) (a) and thickness $h(t)$ (rescaled by the diffusion length $\lambda_{\rm d}$) of the product-rich layer (b) are shown as a function of time for $\sigma_\perp/\sigma_{\rm p}=0.0$ (black), 0.1 (magenta), and 1.0 (light green). The solid and broken lines denote marginal and diffusion-limited regimes, respectively. The results were obtained by numerically integrating Eqs. (5) and (6) with $\alpha=0.01$, $\beta=10.0$, and $L_0/\lambda_{\rm d}=50.0$. The characteristic times at the marginal/diffusion-limited crossover are indicated by dotted lines.

In the marginal regime, the reaction rate continues to follow Eq. (16), even for $t>t_{\rm c}$, because the reaction rate depends only on the local reactant volume fractions determined by thermodynamic equilibrium conditions. In contrast, the thickness $h(t)$ of the product-rich layer for $t>t_{\rm c}$ is expressed as follows:

$$\frac{h_{\rm m}(t)}{\lambda_{\rm d}}=\left(\frac{\alpha\sigma_{\rm p}}{\sigma_\perp}\right)^{\frac{1}{3}}\exp\left(\frac{t}{3\tau_{\rm p}}\right). \tag{20}$$

Equation (20) shows that the thickness $h(t)$ decreases with increasing applied mechanical stress and grows much more slowly than in the absence of material flow (see Table 6). At first glance, one may think that the contribution of material flow to the thickness $h(t)$ may not be important in the marginal regime because it does not affect the reaction rate (Eq. (16)). However, the material flow affects the characteristic time at the crossover between marginal and diffusion-limited regimes because the reaction rate is continuous at the crossover, while the reaction rate depends on the thickness of the product-rich layer in the diffusion-limited regime.

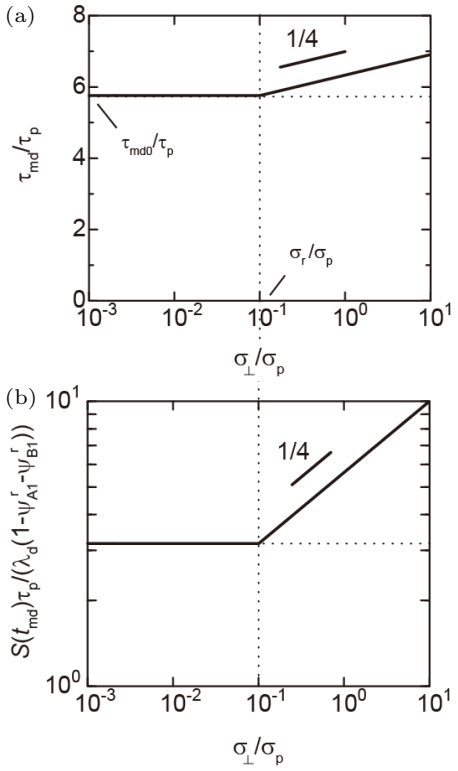


Fig. 5. Marginal/diffusion-limited crossover time vs. applied mechanical stress. Characteristic time t_{md} (rescaled by the time scale τ_p) (a) and reaction rate $S(t_{md})$ (rescaled by the scale S_p) (b) at the marginal/diffusion-limited crossover as a function of applied mechanical stress. Results were obtained using Eqs. (18) and (23) for $\alpha = 0.01$ and $\beta = 10.0$. Slopes of $1/4$ are indicated using short line segments.

In the diffusion-limited regime, the reaction rate is constant for $t > t_c$ and is derived as

$$S_d(t) = D_B \frac{\psi^d_{B1}}{\lambda_d} \left(\frac{\sigma_\perp}{\beta\sigma_p}\right)^{\frac{1}{4}}, \tag{21}$$

by solving Eq. (17) with Eqs. (4) and (9) (broken magenta and light-green lines in Fig. 4(a)). Thus, the reaction rate increases with increasing applied mechanical stress. The acceleration of the diffusion-limited reaction by applied mechanical stress results from the fact that the thickness $h(t)$ of the product-rich layer decreases with increasing stress

$$\frac{h(t)}{\lambda_d} = \left(\frac{\beta\sigma_p}{\sigma_\perp}\right)^{\frac{1}{4}}, \tag{22}$$

(broken magenta and light-green lines in Fig. 4(b)).[32]

When the time t_{md} at the marginal/diffusion-limited crossover is shorter than the characteristic time t_c, the stress-driven material flow is not significant at t_{md}. In this case, the crossover time is given by Eq. (18), $t_{md} = t_{md0}$ (Fig. 5(a)). When $t_{md} > t_c$, the crossover time t_{md} is expressed as

$$\frac{t_{md}}{\tau_p} = \log\left(\frac{\beta^{3/4}\sigma_\perp^{1/4}}{\alpha\sigma_p^{1/4}}\right), \tag{23}$$

which is derived from the continuity of the reaction rate and thickness of the product-rich layer at t_{md} (see Eqs. (20) and (22)). Thus, the characteristic time t_{md} is independent of the applied mechanical stress for small stress and increases with increasing stress magnitude for large stress (Fig. 5(a)). The characteristic stress σ_c at the crossover has the asymptotic form σ_p/β for $\beta/\alpha^2 \gg 1$, when dissolution of reactant A in reactant B-rich solid is smaller than that in the product-rich layer, and, otherwise, $\alpha^4\sigma_p/\beta^3$ for $\beta/\alpha^2 \ll 1$, see the discussion below Eq. (22). The maximum reaction rate $S(t_{md})$ is independent of the applied mechanical stress for $\sigma_\perp < \sigma_c$, but exhibits a power-law dependence on the applied mechanical stress with exponent 1/4 for $\sigma_\perp > \sigma_c$ (Fig. 5(b)). These scaling relationships may be experimentally accessible.

6. Trajectories of regimes with applied mechanical stress

In the absence of applied mechanical stress, the thickness $h(t)$ of the product-rich layer increases over time while the system size remains constant, $L(t) = L_0$. For $L_0 > L_2^*$, the mechanochemical reaction starts in the marginal regime and then shows a crossover to the diffusion-limited regime. Under applied mechanical stress, the stress-driven material flow decreases both the thickness $h(t)$ of the product-rich layer and the system size $L(t)$, because material from the product-rich layer flows out of the system (Fig. 6(a)). Interestingly, under very large applied mechanical stress, the mechanochemical reaction completes before the system reaches the diffusion-limited regime, even for $L_0 > L_2^*$ (magenta arrow in Fig. 6(a)), although the thickness h_{md} of the product-rich layer decreases with increasing applied mechanical stress (broken lines in Fig. 6(a)). In this case, the system instead shows a crossover to the reaction-limited regime. The rate-limiting processes of mechanochemical reactions therefore depend not only on applied mechanical stress but also on the diffusion length λ_d and dissolution of reactant molecules in the product-rich layer.

In the marginal and reaction-limited regimes, the reaction rate is independent of the stress-driven material flow. The fact that the system shows a crossover to the reaction-limited regime rather than the diffusion-limited regime under large mechanical stress implies that the acceleration of the reaction

by mechanical stress has a limitation. The analysis of the reaction trajectories, involving five regimes, is summarized in the SI. For $L_0 > L_2^*$ and $\alpha < \beta^{1/2}$, the trajectory analysis predicts that the crossover switches at a threshold applied mechanical stress

$$\sigma_{\rm th} = \frac{(L_0 - \alpha\lambda_{\rm d})^4}{\beta^3 \lambda_{\rm d}^4}\sigma_{\rm p}, \tag{24}$$

see also Eq. S53 in the SI. The threshold stress is sensitive to the initial size L_0 of the reactant particles. This crossover may be particularly relevant for systems with small reactant particles, and the switching of crossovers may thus be relevant when these particles are relatively small.

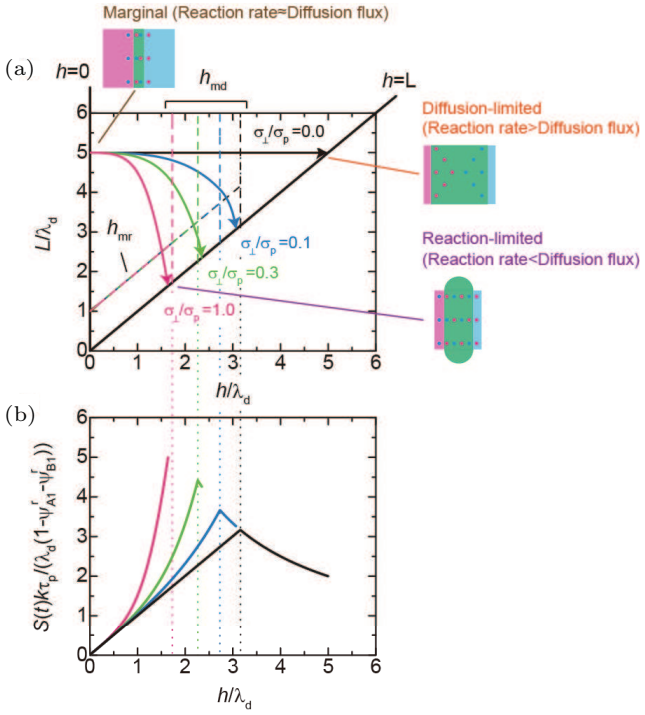


Fig. 6. Reaction trajectories vs. applied mechanical stress. Trajectories (a) and reaction rates $S(t)$ (b) of mechanochemical reactions are shown for $\sigma_\perp/\sigma_{\rm p} = 0.0$ (black), 0.1 (cyan), 0.3 (light green), and 1.0 (magenta) as a function of the product-rich layer thickness $h(t)$ and the system size $L(t)$. The results were obtained by numerically integrating Eqs. (5) and (6) with $\alpha = 0.01$, $\beta = 10.0$, and $L_0/\lambda_{\rm d} = 5.0$. The dotted lines correspond to crossover boundaries separating marginal, diffusion-limited, and reaction-limited regimes (see also Fig. 3).

7. Discussion

We have developed a scaling theory to study the rate-limiting processes of mechanochemical reactions. These processes depend on the thicknesses of the product-rich layer $h(t)$ and the system size $L(t)$, both of which change during the reaction. Our theory predicts that the rate-limiting processes are determined not only by the diffusion length $\lambda_{\rm d}$, but also by the parameters α and β, involved in the dissolution of reactant molecules in the product-rich layer and by the applied mechanical stress $\sigma_\perp$. The trajectories of the system depend on the initial size of the reactant particles and the magnitude of the applied mechanical stress. Stress-driven material flow accelerates the diffusion of reactant molecules in the product-rich layer. Thus, the characteristic time at the marginal/diffusion-limited crossover increases with increasing applied mechanical stress. Under sufficiently large stress, it switches to the marginal/reaction-limited crossover. Our previous theory was limited to relatively small applied mechanical stresses and large time scales, where the mechanochemical reaction is diffusion-limited.[32] The present theory extends this framework to a wider range of applied mechanical stresses and time scales by explicitly considering the crossover between reaction regimes.

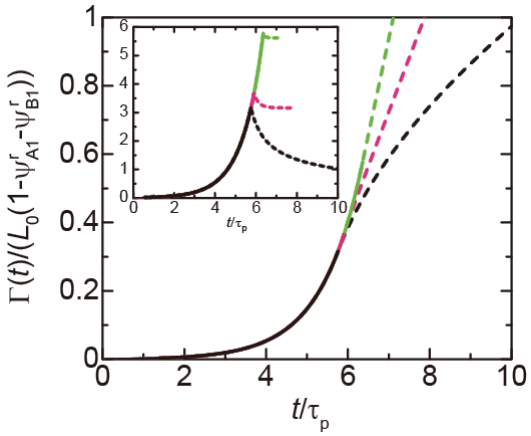


Fig. 7. Conversion ratio vs. time. The conversion ratios $\Gamma(t)/L_0$ (rescaled by the product volume fraction $1 - \psi_{\rm A1}^{\rm r} - \psi_{\rm B1}^{\rm r} \approx 1$ in the product-rich phase) are shown as a function of rescaled time $t/\tau_{\rm p}$ for $\sigma_\perp/\sigma_{\rm p} = 0.0$ (black), 0.1 (magenta), and 1.0 (light green) with $\alpha = 0.01$, $\beta = 10.0$, and $L_0/\lambda_{\rm d} = 10.0$. The rescaled conversion ratio $\Gamma(t)/L_0$ is derived by integrating the rescaled reaction rate $S(t)\,\tau_{\rm p}/[\lambda_{\rm d}(1 - \psi_{\rm A1}^{\rm r} - \psi_{\rm B1}^{\rm r})]$ (shown in the inset) with respect to the rescaled time $t/\tau_{\rm p}$, and then dividing by the rescaled system thickness $L_0/\lambda_{\rm d}$.

Our theory produces a couple of experimentally accessible predictions: First, the mechanochemical reaction accelerates over time on short time scales (marginal regime) and then approaches a constant rate on long time scales (diffusion-limited regime) when the particle size L_0 is larger than the diffusion length $\lambda_{\rm d}$. Second, the reaction rate increases with increasing magnitude of applied mechanical stress mainly on long time scales (see Figs. 4 and 7). These predictions are, at least qualitatively, consistent with the features of the reaction kinetics measured experimentally.[36,37] Our theory further predicts that: 1. the dependence of the reaction rate on the magnitude of the applied mechanical stress in the long-time regime follows a power law with exponent 1/4 (see also Fig. 5); and 2. this acceleration of the mechanochemical reaction saturates when the applied mechanical stress is very large (see also Fig. 6). These experiments may be accessible via quantitative measurements of reaction kinetics over a wide range of applied mechanical stress.

Our scaling theory predicts the thickness $h(t)$ of the product-rich layer and the reaction rate $S(t)$ as functions of

time up to numerical constants of order unity by neglecting higher-order terms. Numerical simulation of Eqs. (2) and (3) including convection is another approach to predict the kinetics of mechanochemical reactions. The latter approach takes into account both reaction and diffusion and thus can predict the reaction rate more precisely and seamlessly. The scaling theory is useful for understanding the physics involved in the kinetics of mechanochemical reactions and for predicting the dependence of the reaction rate on parameters involved in dissolution and rheology.

The main assumption of the present theory is that a small volume of added solvent acts as a plasticizer for the product-rich layer. In our scaling theory, the rheological property of the product-rich phase is represented by its viscosity η_{AB} (Eq. (4)). The extent of softening depends on the compounds and volume of the added solvent, in contrast to the hot-spot theory,[38–41] which predicts that mechanical stresses locally increase the temperature for a short period of time. The present theory predicts that even a solvent that selectively dissolves the product molecules, but not the reactant molecules, enhances reactivity. Experimentally measuring the reactivity and rheology by changing solvent and its volume can provide further insights into the mechanisms of solvent-mediated reactivity enhancement in mechanochemical systems.

The present theory is limited to analysis at the interfacial length scales. The macroscopic dynamics of the reactant particles and milling balls during ball milling break and mix the solid particles, making the applied mechanical stress time-dependent. From the viewpoint of interfacial length scales, mechanical agitation breaks the reactant particles to create new surfaces (and also changes the system size $L(t)$) and exchanges the pairs of particles forming the interfaces. Among these effects, the creation of new surfaces by particle breakage can be a rate-limiting process for binary reactions. Our present theory assumes that reactant particles are rigid bodies, and the mechanism of reaction acceleration predicted by this theory differs from mechanisms involving the creation of new interfaces, which is usually considered the mechanism of mechanical mixing. Interestingly, pre-milling of reactant particles does not change the kinetics of mechanochemical reactions in some experiments.[36,42] The present theory is best tested by such experiments.

The present theory integrates the microscopic dynamics of atoms during chemical reactions into our mesoscopic approach, focusing on the dynamics of molecules at interfaces via the kinetic constant k, but does not address how the kinetic constant k depends on applied mechanical stress. At first glance, applied mechanical stress might be expected to decrease the activation barrier through the work done by atomic displacements. However, in general, these effects are thought to be weak for reactions between small molecules. Nevertheless, applied mechanical stress can potentially change the statistical weight of reactant conformers, which may be significant in certain reactions.

8. Conclusion

The theory predicts that mechanochemical reactions exhibit rich crossovers of rate-limiting processes, in contrast to conventional solution-phase reactions. The reaction rate constant k, which can be estimated by quantum chemical calculations, is integrated into mesoscopic molecular behavior at interfaces, thus marking the first step toward bridging molecular and mesoscopic theories. Our present theory is limited to cases in which: 1. the reaction is of type $\mathrm{A}+\mathrm{B}\rightarrow\mathrm{AB}$; 2. the reactant solids A and B do not form eutectic systems; 3. the reactant solids act as rigid bodies and the product-rich phase acts as a Newtonian fluid; and 4. the system is isothermal. However, this theory takes into account dissolution, diffusion, rheology, and chemical reaction and thus can be extended to the cases of different reaction types,[11,42] miscibility, mechanical properties, and ensembles.[36] We believe that critical experimental tests of our present theory will advance our understanding of the kinetics of mechanochemical reactions under ball milling.

Data and code availability

The Mathematica notebook file used for the numerical calculations and the data are available on figshare with the identifier (https://doi.org/10.6084/m9.figshare.30383023).

Acknowledgments

Project supported by JSPS KAKENHI (Grant Nos. 24H00453, 24H01832, 24H01050, 22K18333, and 22H00318), by JST CREST (Grant No. JPMJCR19R1), and by JST FOREST (Grant Nos. JPMJFR201I and JPMJFR2221). The Institute for Chemical Reaction Design and Discovery (ICReDD), which has been established under the World Premier International Research Initiative (WPI), MEXT, Japan. T. Y. is grateful to Masao Doi, Yuichi Masubuchi, and Shunto Arai for fruitful discussions.

References

[1] James S L, Adams C J, Bolm C, Braga D, Collier P, Friščić T, Grepioni F, Harris K D M, Hyett G, Jones W, Krebs A, Mack J, Maini L, Orpen A G, Parkin I P, Shearouse W C, Steed J W and Waddell D C 2012 *Chem. Soc. Rev.* **41** 413
[2] Do J L and Friščić T 2017 *ACS Cent. Sci.* **3** 13
[3] Hernández J G and Bolm C 2017 *J. Org. Chem.* **82** 4007
[4] Tan D and Garcia F 2019 *Chem. Soc. Rev.* **48** 2274
[5] Kubota K and Ito H 2020 *Trends in Chem.* **2** 1066
[6] Kubota K 2023 *Bull. Chem. Soc. Jpn.* **96** 913
[7] Speight I R, Ardila-Fierro K J, Hernández J G, Emmerling F, Michalchuk A A L, García F, Colacino E and Mack J 2025 *Nat. Rev. Methods Primers* **5** 29

[8] Seo T, Toyoshima N, Kubota K and Ito H 2021 *J. Am. Chem. Soc.* **143** 6165

[9] Do J L, Mottillo C, Tan D, Štrukil V and Friščić T 2015 *J. Am. Chem. Soc.* **137** 2476

[10] Zholdassov Y S, Kwok R W, Shlain M A, Patel M, Marianski M and Braunschweig A B 2024 *RSC Mechanochem.* **1** 11

[11] Vugrin L, Carta M, Lukin S, Meštrović E, Delogu F and Halasz I 2023 *Faraday Discuss.* **241** 217

[12] Urakaev F Kh and Boldyrev V V 2000 *Powder Technology* **107** 93

[13] Polo A, Carta M, Delogu F, Rustici M and Budroni M A 2022 *Front. Chem.* **10** 915217

[14] Nunez S G, Schott D L and Padding J T 2025 *Powder Technology* **457** 120919

[15] Carta M, Delogu F and Porcheddu A 2021 *Phys. Chem. Chem. Phys.* **23** 14178

[16] Li J, Nagamani C and Moore J S 2015 *Acc. Chem. Res.* **48** 2181

[17] Wiggins K M, Brantley J N and Bielawski C W 2012 *ACS Macro. Lett.* **1** 623

[18] Mu Q and Hu J 2024 *Phys. Chem. Chem. Phys.* **26** 679

[19] Kubota K, Toyoshima N, Miura D, Jiang J, Maeda S, Jin M and Ito H 2021 *Angew. Chem. Int. Ed.* **60** 16003

[20] Kubota K, Jiang J, Kamakura Y, Hisazumi R, Endo T, Miura D, Kubo S, Maeda S and Ito H 2024 *J. Am. Chem. Soc.* **146** 1062

[21] Jiang J, Kubota K, Harabuchi Y, Jin M, Wang Z J, Nakajima T, Ito H, Gong J P and Maeda S 2025 *J. Am. Chem. Soc.* **147** 32502

[22] Beyer M K 2000 *J. Chem. Phys.* **112** 7307

[23] Klen I M, Husic C C, Kovács D P, Choquette N J and Robb M J 2020 *J. Am. Chem. Soc.* **142** 16364

[24] Ribas-Arino J, Shiga M and Marx D 2009 *Angew. Chem. Int. Ed.* **48** 4190

[25] Zholdassov Y S, Yuan L, Garcia S R, Kwok R W, Boscoboinik A, Valles D J, Marianski M, Martini A, Carpick R W and Braunschweig A B 2023 *Science* **380** 1053

[26] Yan H, Yang F, Pan D, Lin Y, Hohman J N, Solis-Ibarra D, Li F H, Dahl J E P, Carlson R M K, Tkachenko B A, Fokin A A, Schreiner P R, Galli G, Mao W L, Shen Z X and Melosh N A 2018 *Nature* **554** 505

[27] Wang Y, Dong X, Tang X, Zheng H, Li K, Lin X, Fang L, Sun G, Chen X, Xie L, Bull C L, Funnell N P, Hattori T, Sano-Furukawa A, Chen J, Hensley D K, Cody G D, Ren Y, Lee H H and Mao H 2019 *Angew. Chem. Int. Ed.* **58** 1468

[28] Ferguson M, Moyano M S, Tribello G A, Crawford D E, Bringa E M, James S L, Kohanoff J and Pópolo M G D 2019 *Chem. Sci.* **10** 2924

[29] Ferguson M and Friščić T 2024 *Phys. Chem. Chem. Phys.* **26** 9940

[30] Yamamoto T, Kubota K and Ito H 2024 *J. Soc. Rheol. Jpn.* **52** 161

[31] Kubota K, Seo T, Koide K, Hasegawa Y and Ito H 2019 *Nat. Commun.* **10** 111

[32] Yamamoto T, Kubota K, Harabuchi Y and Ito H 2025 *RSC Mechanochemistry* **2** 230

[33] Atkins P, de Paula J and Keeler J 2023 *Physical Chemistry (12th edn.)* (Oxford: Oxford Univ. Press)

[34] Doi M 2013 *Soft Matter Physics* (Oxford, Oxford University Press)

[35] Safran S A 2003 *Statistical Thermodynamics of Surfaces, Interfaces, and Membranes* (Boulder: Westview Press)

[36] Hutchings B P, Crawford D E, Gao L, Hu P and James S L 2017 *Angew. Chem. Int. Ed.* **56** 15252

[37] Julien P A, Malvestiti I and Friščić T 2017 *Beilstein J. Org. Chem.* **13** 2160

[38] Bowden F P and Yoffe A 1952 *Initiation and Growth of Explosion in Liquids and Solids* (Cambridge: Cambridge University Press)

[39] Bowden F P and Yoffe A 1958 *Fast Reactions in Solids* (London: Butterworths)

[40] Bowden F P and Tabor D 1958 *The Friction and Lubrication of Solids* (Oxford: Clarendon Press)

[41] Delogu F and Cocco G 2008 *J. Alloys Compd.* **465** 540

[42] Ardila-Fierro K J, Lukin S, Etter M, Užarević K, Halasz I, Bolm C and Hernández J G 2020 *Angew. Chem. Int. Ed.* **59** 13458